JJ

GSI

GSI-Preprint-97- 41
August 1997

RECOIL ION MOMENTUM SPECTROSCOPY

J. Ullrich, W. Schmitt, R. Dörner, O.Jagutzki, V. Mergel, R. Moshammer,
H. Schmidt-Böcking, L. Spielberger, M. Unverzagt, R. E. Olson

(Plenary Lecture, XX. ICPEAC in Vienna, July 23-29, 1997)

Gesellschaft für Schwerionenforschung mbH
Planckstraße 1 • D-64291 Darmstadt • Germany
Postfach 11 05 52 • D-64220 Darmstadt • Germany

RECOIL ION MOMENTUM SPECTROSCOPY

J. ULLRICH, W. SCHMITT

Gesellschaft für Schwerionenforschung mbH, Planckstr. 1, D-64291 Darmstadt, Germany

R. DÖRNER, O. JAGUTZKI, V. MERGEL, R. MOSHAMMER, H. SCHMIDT-BÖCKING, L. SPIELBERGER, M. UNVERZAGT

Institut für Kernphysik, Universität Frankfurt, August-Euler Str. 6, D-60486 Frankfurt

R.E. OLSON

University of Missouri-Rolla, Department of Physics, Rolla, Missouri 65401, USA

High-resolution **R**ecoil-**I**on **M**omentum **S**pectroscopy (RIMS) is a novel technique to determine the charge state and the complete final state momentum vector $\mathbf{P_R}$ of a target ion recoiling from an ionising collision of any kind of radiation with a target atom. It offers a unique combination of superior momentum resolution in all three spatial directions of $\Delta P_R = 0.07$ a.u. with a large detection solid angle of $\Delta\Omega_R/4\pi \geq 98$ %. Recently, low-energy electron analysers based on rigorously new concepts and reaching similar specifications were successfully integrated into RIM spectrometers yielding so-called „reaction microscopes".
Exploiting these techniques, a large variety of atomic reactions for ion, electron, photon and antiproton impact have been explored in unprecedented detail and completeness and will be highlighted in this article. Emphasis is given to envisage the rich future potential of the method in various fields of atomic collision physics with atoms, molecules and clusters.

1. Introduction

The kinematically complete experimental investigation as well as a theoretical description of atomic many-particle scattering dynamics still face basic problems. This is in striking contrast to the outstanding precision having been achieved in the understanding of the static structure of atoms. Even for one of the most „simple" three-particle situations, namely single ionisation of hydrogen or helium atoms by low-energy charged particle or antiparticle impact a complete experiment has not been available until the advent of Recoil-Ion Momentum Spectroscopy. The classical trajectory Monte Carlo method has been applied but no quantum mechanical theory is at hand (see e.g. Refs. 1,2). So far, kinematically complete experiments have been restricted to single ionisation after electron impact (see e.g. Ref. 3) or double ionisation as a result of the absorption of a photon (e.g. Refs. 4-6). Theoretically severe difficulties already arise if two active target electrons are involved as for double ionisation of helium in collisions with photons, ions or electrons (see e.g. Ref. 7).

One reason for the lack of data is the extreme small product solid angle of conventional electron spectrometers for the coincident detection of two continuum electrons of $\Delta\Omega_{ee}/4\pi \approx 10^{-4} - 10^{-7}$. Only two pioneering studies for favorable kinematics have been reported where three electrons were analyzed simultaneously[8]. For ion-

impact a second, major complication arises in that the typical relative momentum change of the projectile $\Delta P_P/P_P$ is on the order of $10^{-4} \leq \Delta P_P/P_P \leq 10^{-9}$ and therefore is not accessible experimentally. Consequently, no kinematically complete experiment on single ionisation in ion-atom collisions has been performed until recently.

Recoil-Ion Momentum Spectroscopy (RIMS) has been developed over more than a decade in order to overcome this fundamental problem and to provide an efficient and precise experimental tool to explore the correlated dynamics of collision induced atomic many-particle reactions. After a brief overview on the history of development and the basic concepts of RIMS in section 2 a short summary of the kinematics of recoil-ion production is given in section 3. Some of the most prominent recent results achieved using RIMS are highlighted in section 4. This selection can by far not be complete due to the limited scope of this paper and the reader is referred to the reviews by Cocke and Olson[9] 1991 and by Ullrich et al[10] 1997.

2. From Recoil-Ion Momentum Spectroscopy to „Reaction Microscopes"

Apart from early measurements in the 60's and 70's by Federenko and Afrosimov[11], as well as Everhart and Kessel[12] and by McConkey et al.[13] the recoiling target ion momentum has practically not been accessed by the experimentalists for a long time. The reason being the extremely small energies transferred to the target nucleus during most of the atomic reactions for charged particle or photon impact. Due to the large mass of the nucleus compared to the electron mass recoil-energies E_R are typically well below 1 eV ranging into the μeV and even sub-μeV regime for a majority of atomic reactions.

2.1 Early Time-of-Flight Spectrometers

In the late 80's a few groups at Oak-Ridge[14], Frankfurt[15] and Caen[16] reported on successful attempts to detect such ions and obtained information on their mean energies. At the same time Ullrich and Schmidt-Böcking in Frankfurt were the first to actually measure the recoil-ion momenta[17,18] using static, spatially extended targets at room temperature with a resolution limited by the target thermal motion at 300 K ($\Delta E_R \approx$ 40 meV). This first recoil-ion momentum spectrometer is shown in Fig.1. Target ions were created along the ion beam on the axis of a cylindrically shaped, extended target cell („inner cylinder" of 5 mm radius and 40 mm length). They drifted from the axis towards the walls of the cylinder during a time interval inversely proportional to their transverse velocity gained within the collision (transverse to the ion beam propagation). After acceleration between the inner and outer cylinders, the recoil ions were focused by an Einzel-lens, charge state analysed in a magnetic field and detected by a position sensitive micro-channel plate (MCP). From the ion time-of-flight (TOF) the transverse momentum was obtained for different recoil-ion charge states (positions on the detector). Later, in an improved version, the inner cylinder

was cooled to 30 K resulting in an increased energy resolution of $\Delta E_R \approx 4$ meV[19,20]. Recoil-ion momenta transverse to the incoming projectile momentum were measurable and solid angles of up to a few percent of 4π were obtained.

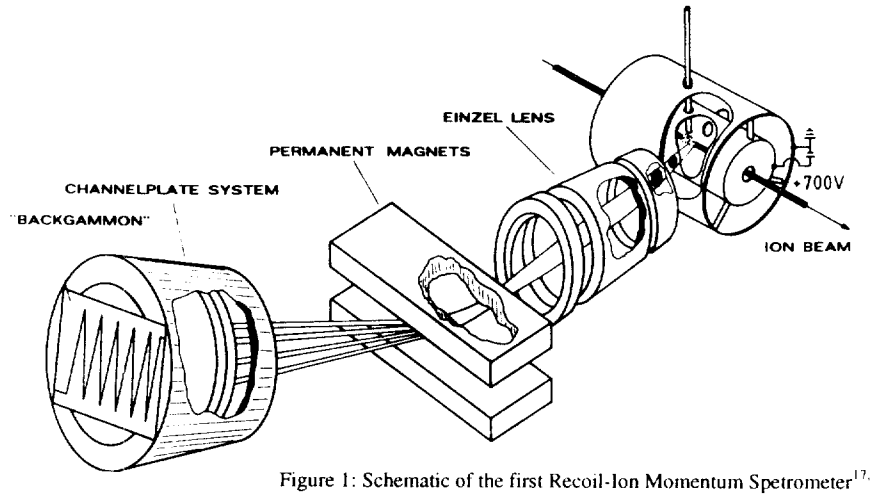

Figure 1: Schematic of the first Recoil-Ion Momentum Spetrometer[17,18]

Exploiting inverse kinematics, scattering angles of heavy projectiles in the microradian regime became indirectly accessible and the first experimental investigations of transverse momentum exchanges for ionisation, electron capture and transfer ionisation reactions were performed[15,20-26].

2.2 Modern High-Resolution RIM Spectrometers

Rapid progress was initialised by implementing localised gas-jet targets in connection with recoil-ion projection techniques at Kansas State University, CIRIL in Caen and Frankfurt. Recoil-ions created in the intersection volume between the localised gas-target and the ion-beam were extracted by an electrostatic field and projected onto position sensitive detectors[27-31] (for a recent, improved set-up see e.g. Fig.2). By measuring the flight times and the positions of the ion impact on the detector, their trajectories can be reconstructed in an unambiguous way for each ion charge state and the complete initial momentum vectors can be calculated. A tremendous increase in solid angle to values of nearly 100% of 4π was realised by this concept and a similar resolution as with the cooled static targets was obtained using „warm" effusive jets[27-29, 36,37]. Internally cold supersonic atomic jets developed parallel in Caen and Frankfurt paved the way to a dramatic increase in momentum resolution corresponding to energy resolutions far below 1 meV[30,31]. Precooling of the target gas before the supersonic expansion pushed the resolution to a few μeV for helium-ions and was termed cold target recoil-ion momentum spectroscopy: COLTRIMS[32,33].

Using focusing electrostatic extraction fields[55] the development recently culminated in a superior resolution of $\Delta E_R \approx \pm 1.2$ μeV for He^{1+} ions with a solid angle of 4π for the detection of momenta below 5 a.u.[34].

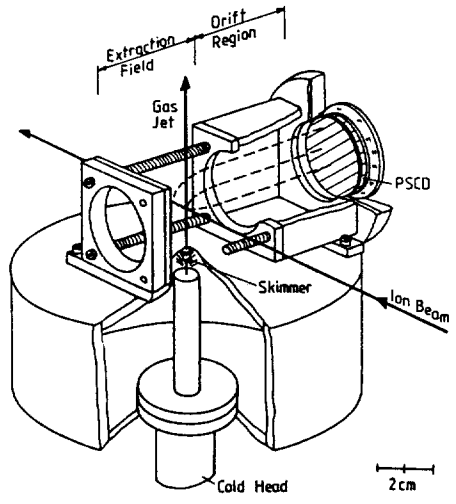

Figure 2: Modern RIM spectrometer with a supersonic jet, homogeneous or lens-like extraction field into the transverse direction, drift region for time-focusing and position sensitive detection of the ions.

This device, developed in Frankfurt is shown in Fig. 2. Here, the rare gas is precooled to a temperature of approximately 15 K (for He) at a pressure between 200 and 1000 mbar using a cryogenic cold head. The gas then expands through a 30 μm hole forming a supersonic jet. The inner jet fraction passes through a 0.3 mm skimmer into the scattering chamber yielding an atomic beam with a diameter of about 1 mm at the intersection point with the projectile beam. The internal momentum spread of the target in the direction of the gas jet is determined by the parameters of the expansion and is typically below ±0.05 a.u.. In the direction transverse to the jet expansion an even smaller momentum spread between ±0.015 a.u. and ±0.035 a.u. is achieved by skimming of the atomic beam. In order to provide precisely controlled extraction fields for the recoil-ions a 10 m long 7 μm carbon fiber was wound around four supporting germanium coated isolator screws. Recently, non homogeneous, lens-like extraction fields E_{ex} have been developed[55]. They guide ions which emerge with identical momenta from different positions in the two-dimensional plane transverse to the extraction field within the interaction volume to the same position on the channel plate. Thus, the momentum resolution in the two dimensions perpendicular to the extraction is no longer restricted by the uncertainty of the starting positions. In all spectrometers a drift region follows the extraction field (see Fig. 2). Its length is adapted to the length and form of E_{ex} in such a way, that the ions created with the same momentum but at different positions along the field within the interaction volume arrive at the same time at the detector („time focusing"). Combining both con-

cepts, spectrometers which focus in all three spatial dimensions have become feasible and the uncertainty in the momentum measurement due to the finite size of the interaction volume becomes negligibly small.

With these spectrometers the complete momentum vector of one reaction product, the target ion, emerging from any ionising atomic collision was measurable with a resolution of a few percent and a solid angle of nearly 100% of 4 π. Experiments became feasible where contributions to the projectile ionisation due to the electron-nucleus or electron-electron interaction were kinematically separated[35,36]. Studies of the scattering angle dependence of single and double electron capture into different shells of the projectile at medium velocities were performed[32,37-41]. „Transfer ionisation" in proton-helium collisions (one helium electron is captured by the projectile the other one is emitted) was investigated in kinematically complete experiments[42]. The contributions of photoabsorption and Compton scattering to He double ionisation at high photon energies became separable[43,44].

2.3 „Reaction - Microscopes"

The latest tremendous step forward, opening a new era of future investigations even beyond „conventional" RIMS was achieved at GSI: A high-resolution RIM spectrometer, based on a precooled supersonic jet (COLTRIMS) was combined with an innovative low-energy electron analyser where the basic principles of the recoil-ion detection were now applied to the electrons. They are efficiently projected onto a position sensitive detector by a combination of electrostatic and solenoidal magnetic fields[45]. In most recent arrangements, termed „Reaction Microscopes", the complete momentum vectors of up to three electrons with energies below 50 eV can be determined simultaneously (in addition to the recoil-ion) using three independent electron detectors (see Fig. 3). A momentum resolution for the electrons of $\Delta P_e \approx \pm 0.02$ a.u. has been achieved corresponding to an electron energy resolution of $\Delta E_e \approx \pm 5$ meV. Using these or similar „reaction microscopes", kinematically complete experiments have been performed for single and double ionisation of helium after ion impact[34,46,47] as well as for He double photoionisation close to threshold[48,49].

In the most recent GSI Reaction-Microscope shown in Fig. 3, ions and electrons are usually extracted into the longitudinal direction (along the projectile beam) by generating the extraction field between two ceramic plates. Each ceramic is plated with two burned-in resistive layers with different resistances in such a way that any direction of the electrostatic field vector can be generated (in the transverse or longitudinal or any other direction; details are given in Refs. 45, 50). Voltages can be applied such that position-focusing electrostatic fields are generated for the transverse momentum components. The longitudinal momentum component containing the most important information for ion-impact (the inelasticity, see next section) is time-focused. Total extraction voltages typically range up to +100 V. Thus, all

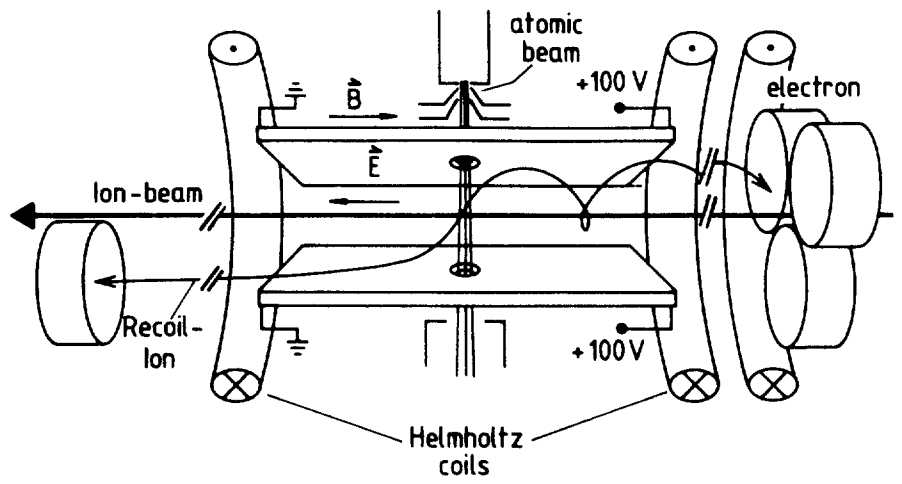

Figure 3: Schematic of the GSI Reaction-Microscope[45].

electrons with longitudinal forward energies of $E_{e\|} \leq 50$ eV are accelerated upstream hitting one of the three position sensitive MCPs. The electron detectors are placed in the backward direction in time-focusing geometry at a total flight path of 33 cm. By applying a weak solenoidal magnetic field (12 Gauss) with its axis slightly tilted to the beam direction all electrons with non-zero transverse energies $E_{e\perp}$ are forced into spiral trajectories and projected on the detectors with a 4π solid angle for $E_{e\perp} \leq 50$ eV. The electron longitudinal momenta are obtained from their times-of-flight (TOF), measured in a coincidence between each of the electrons, the projectile and the recoil ion. The position contains the information on the transverse momentum and on the azimuthal emission angle. Thus, the complete momentum vector of up to 3 electrons has been determined simultaneously and a solid angle close to 4π was reached for all electrons with $E_e \leq 50$ eV. The momentum resolution of the latest apparatus has been discussed by Kollmus and a resolution of $\Delta P_e = \pm 1 \cdot 10^{-2}$ a.u. corresponding to an energy resolution $\Delta E_e = \pm 1.4$ meV (at $E_e = 0$ eV) has been estimated. Very recently, one of the detectors was equipped with a fast position sensitive delay-line readout[51,52]. Using a fast multi-hit time-to-amplitude converter, up to 16 electrons emerging from one single collision can be accepted and for each of them the complete momentum vector can be calculated.

More recently, another concept, well adapted to detect low-energy electrons ($E_e \leq 10$ eV) in combination with high-resolution RIMS was used by Dörner[47,49] placing a position sensitive detector for the emitted electrons in the direct vicinity of the interaction volume opposite to the recoil-ion detector.

3. Kinematics

In this section a short summary of the non-relativistic kinematics will be given (for details see e.g. Refs. 18,53-55). Throughout this paper atomic units are used where the electron mass m_e, the electron charge e and the Planck constant $\hbar$ is equal unity.

3.1. Ion-Atom Collisions

For the overwhelming part of all atomic reactions in ion-atom collisions, only a small fraction of the initial momentum (P_P), energy (E_P) and mass (M_P) of the incoming projectile is transferred during the encounter. Also, the momenta of emitted photons are typically small and will be neglected. Under these conditions the longitudinal and transverse momentum balances are decoupled[17], contain different kinematical information on the collision and can be calculated separately on the basis of non-relativistic energy and momentum conservation.

- In the <u>transverse direction</u> one obtains for the final momenta of the recoil-ion ($\mathbf{P}_{R\perp}$), the projectile ($\mathbf{P}_{P\perp}$) and the electrons ($\Sigma\mathbf{P}^i_{e\perp}$) in the laboratory frame (bold letters denote vectors):

$$\mathbf{P}_{R\perp} = -(\mathbf{P}_{P\perp} + \Sigma\mathbf{P}^i_{e\perp}). \tag{1}$$

For reactions with no electrons in the continuum (pure electron capture) or those where $\Sigma\mathbf{P}^i_{e\perp}$ is small compared to the heavy particle momenta (i.e. at small impact parameters or for collisions at small projectile energies), one obtains $\mathbf{P}_{R\perp} \approx \mathbf{P}_{P\perp}$. In this case the transverse recoil-ion momentum results from the repulsive inter-nuclear scattering and an impact parameter can be calculated for a given deflection potential[21,22,25,47]. For ionisation reactions at medium and high projectile velocities the transverse momenta of all reaction products are usually of the same order of magnitude so that the full many-body momentum exchange has to be considered.

- In the <u>longitudinal direction</u> one obtains:

$$P_{R\parallel} = -(\Delta P_{P\parallel} + \Sigma P^i_{e\parallel}) \tag{2}$$

where
$$\Delta P_{P\parallel} = \Delta E_P/v_P = -Q/v_P + \tfrac{1}{2}\, n_e \cdot v_P - \Sigma E^i_e/v_P \tag{2a}$$

$\Delta P_{P\parallel} = \Delta E_P/v_P$ denotes the momentum change of the projectile in the longitudinal direction and can be related to the energy change of the projectile ΔE_P with the initial velocity v_P. n_e is the numbers of electrons transferred from the target to the projectile. Q is the change in internal energy of the projectile and the target, i.e. the energy difference between initial and final bound electronic states $Q = E_f^{bind} - E_i^{bind}$ (exothermic reactions yield negative Q-values). E^i_e is the continuum energy of the i^{th} electron in the laboratory frame. Thus, the energy balance of the collision is completely contained in the longitudinal momentum components and information on the Q-value of the reaction as well as on the mass transfer can be obtained by measuring these components alone.

3.2 Collisions with Photons

Only the general features of the kinematics of photon atom collisions are given here. Details have been given by Vogt[56].

• If a photon is absorbed by an atom practically its entire energy is deposited into the target electron shell. Thus, for single photo ionisation, one electron emerges with an energy of $E_e = E_\gamma - E^{bind} - E^{exc}$ having a momentum of $P_e = \sqrt{2E_e}$. This momentum is compensated by the recoiling target ion resulting in P_R-distributions on spheres in momentum space with radii $P_R = P_e$ in the centre of mass system depending on the incident photon energy and the excitation energy of the remaining target electrons. In the laboratory frame the sphere for the ion is shifted along the photon beam direction by $P_{R\|} = P_\gamma = E_\gamma/c$. The intensity distribution on these spheres mirror the angular emission characteristics of the emitted photo electron.

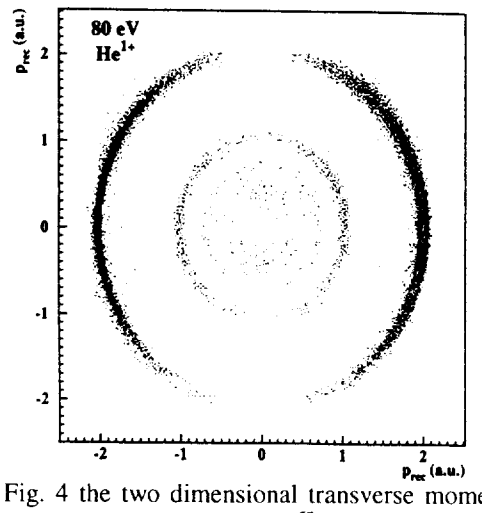

Figure 4: Momentum distribution of He^{1+} ions produced by 80.1 eV photons[57] (note: a different notation for the recoil-ion momenta was used in this publication $P_R = P_{rec}$). The horizontal x-axis is the direction of the electric field vector of the linearly polarised light. The vertical y-axis is the direction of the gas jet. The data are integrated over a momentum range of ±0.1 a.u. in the z-direction, which is the direction of the photon beam.

In Fig. 4 the two dimensional transverse momentum distribution of recoiling He^{1+} ions measured by Dörner et al.[57] is shown for an incident photon energy of $E_\gamma = 80.1$ eV (note: the whole momentum sphere was measured simultaneously and only an illustrative subset is shown in Fig. 4). The longitudinal shift due to the photon momentum of $P_\gamma = 0.022$ a.u. is negligibly small. The various kinematical rings observed are due to different final states of the remaining He^{1+} (outer ring: ground state, second ring: first excited state etc.). Since linearly polarised light (along the x-axis) has been used in this experiment the intensity distribution on the outer ring is given by the dipole emission characteristics of the emerging photo electron (ion). If the second electron is left in an excited state (via ionisation plus excitation or double excitation in the vicinity of a resonance followed by autoionisation), the emitted electron (recoiling target ion) does not display dipole-characteristics which can be efficiently explored using RIMS.

• For Compton scattering the photon can be scattered at a free electron where energy and momentum conservation is fulfilled by the photon and the electron alone ($\mathbf{P}_e = \mathbf{P}_\gamma - \mathbf{P}_{\gamma'}$ and $E_e = E_\gamma - E_{\gamma'}$ for an electron initially at rest in the laboratory system). If the electron is in a bound state the three-body momentum balance has to be considered. For large momentum transfers by the photon the impulse approximation can be applied assuming the bound electron to be quasi free with an initial momentum distribution given by its momentum distribution in the atom ($\mathbf{P}^{in}_e$ with $E^{in}_e = \frac{1}{2}\cdot(P^{in}_e)^2$), i.e. its „Compton profile". This yields $\mathbf{P}_e = \mathbf{P}_\gamma - \mathbf{P}_{\gamma'} + \mathbf{P}^{in}_e$ and from momentum conservation one obtains for single ionisation by Compton scattering:

$$\mathbf{P}_\gamma + \mathbf{P}_{He} = \mathbf{P}_{\gamma'} + \mathbf{P}_R + \mathbf{P}_e \qquad (3)$$

or:
$$\mathbf{P}_R = -\mathbf{P}^{in}_e \qquad (3a)$$

in the approximation that no momentum exchange with the target nucleus occurs in the exit channel, that the initial momentum of the helium atom $\mathbf{P}_{He} \approx 0$ and that the Compton scattering cross section is independent on the electron momentum (all approximations are usually well fulfilled). Then, for ionisation as a result of Compton scattering the target-ion recoil momentum is a broad distribution even for monoenergetic photon impact and mirrors the electron initial state momentum distribution.

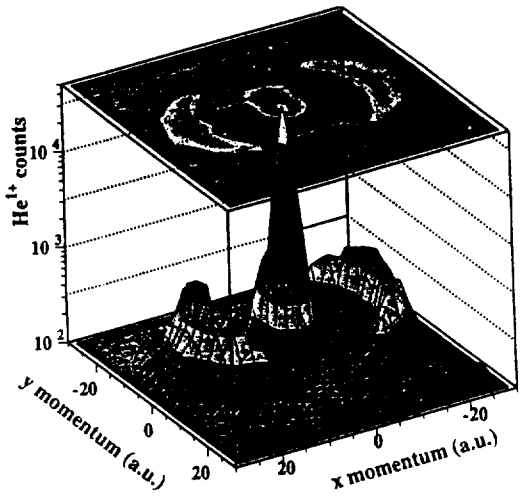

Figure 5: Momentum distribution of He^{1+} ions produced by 8.8 keV photons[43]. The x-axis is the direction of the electric field vector of the linearly polarised light. The y-axis is the direction of the gas jet. The data are integrated over the full momentum range of ±30 a.u. in the z-direction, which is the direction of the photon beam.

Spielberger et al. for the first time directly measured the He^{1+}- and He^{2+}-ion momentum distributions for 8.8 keV photon impact[43]. In addition to the kinematical sphere for photoabsorption with a radius of about 30 a.u. a peak of slow recoil ions was observed which was centred around $\mathbf{P}_R = 0$ a.u. having a width of about 1 a.u. resulting from Compton scattering of the photons (Fig. 5 for He single ionisation).

4. Selected Results

One outstanding feature of RIMS is its applicability for all projectile species at any impact energy as well as the nearly complete independence of the achievable resolution from the energy spread and angular divergence of the projectile beam. This has prompted experiments extending over the whole variety of projectiles and collision energies available. It is far beyond the scope of this article to give a complete overview on atomic collision phenomena investigated using RIMS (for recent reviews see Refs. 9,10). Here, an admittedly subjective choice had to be made and a few kinematically complete studies which represent - from the perspective of the authors- milestone experiments on the different atomic reactions have been selected.

4.1 Single Ionisation by Ion Impact

When energetic charged projectiles interact with neutral atoms, the ejection of one target electron is the dominant reaction channel. Despite of its outstanding importance, no kinematically complete experimental investigation has been published until the advent of RIMS that provides coincident information on the electron emission, the recoil-ion scattering, and the energy loss as well as angular straggling of the projectile. Using the GSI-reaction microscope shown in Fig.3 the complete three particle final state momentum distribution was imaged with a resolution of $\Delta p_i \approx \pm 0.1$ a.u. for single ionisation of He by 3.6 MeV/u Se^{28+} impact[58].

A convenient representation to illuminate the complete three particle momentum balance is to project the momenta of all outgoing reactants onto the collision plane defined by the incident projectile momentum ($P_{\parallel}$ direction) and the transverse recoil-ion momentum vector ($-P_x$ direction) as shown in Fig. 6. Several important features on the dynamics of target single ionisation by ion impact in the regime of strong perturbations can be observed: First low-energy electrons are found to be preferentially scattered in the forward ($+P_{\parallel}$) direction. This has been shown to be a result of a „Post Collision Interaction" (PCI) of the emerging, highly charged projectile „pulling" the low energy continuum electron behind[33,59,60]. At the same time, the positively charged recoiling target ion is pushed to the backwards direction. Going to smaller perturbations this „asymmetry" in the „soft" electron emission vanishes[61] and the distribution becomes symmetric around $P_{\parallel} = 0$.

Second, recoil-ion and electron are preferentially emitted back-to-back balancing their momenta on a level which corresponds to the small momentum ($\Delta \mathbf{P}_P$) transferred by the projectile (right part of Fig. 6). $\Delta \mathbf{P}_P$ is calculated for each single collision from the measured final momenta of the electron and of the recoil ion: $\Delta \mathbf{P}_P = -(\mathbf{P}_R + \mathbf{P}_e)$. This way the energy loss and angular straggling of a fast projectile in a single collision becomes indirectly accessible with an accuracy $\Delta E_P/E_P$ of up to 10^{-9} (for 1 GeV/u U impact) which is orders of magnitude better than achievable in any energy gain or loss measurement using conventional techniques.

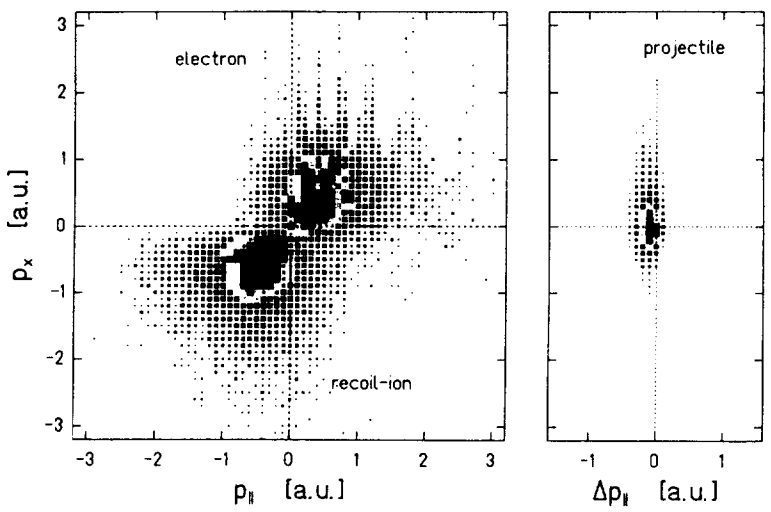

Figure 6: Projections in momentum space of all particles in the final state onto the plane determined by the incident projectile and the outgoing He^{1+} recoil-ion momentum vectors (i.e. the collision plane) for single ionisation of He by 3.6 MeV/u Se^{28+} impact[58]. The cluster size represents the corresponding doubly differential cross section $d^2\sigma/(dP_x dP_y)$ in a logarithmic scale.

For small Q-values and small emitted electron energies E_e at large projectile v_P such a behaviour is formally evident from momentum conservation in the longitudinal direction since $\Delta P_{P\parallel} = -(Q/v_P + E_e/v_P) \approx 0$. Under these conditions it holds that $\Delta P_{P\parallel} \approx \sum P^i_{e\parallel}$ providing a unique possibility to obtain information on the collective behaviour of several electrons emitted in multiple ionisation events. For strong perturbations it was observed at GANIL[62] and GSI[63] for multiple ionisation of Ar and Ne that the ions are thrown backwards prooving that up to 7 electrons are preferentially scattered into the forward direction in such encounters.

It was pointed out recently, that in the limit of projectile velocities approaching the speed of light the longitudinal momentum transfer of the highly charged projectile becomes as small as the momentum transfer by a photon of equivalent energy. Therefore, the fast highly-charged projectile was interpreted[46,64,65] to act like an ultrashort, intense and broad band virtual photon field, dissociating the atom.

Very recently, a second set of highly differential experiments on single ionisation was performed for 5 keV to 15 keV proton impact on helium[47]. Using an similar reaction microscope developed at Frankfurt, the two-dimensional momentum distribution of very low-energy continuum electrons ($E_e \leq 13$ eV) was determined for defined impact parameter and orientation of the scattering plane. Both were obtained from the measured recoil-ion transverse momentum which, for slow collisions reflects the projectile scattering in very good approximation.

4.2 Electron Capture

If there are no electrons in final continuum states equation (2a) reduces to:

$$P_{R\|} = Q/v_P - \tfrac{1}{2}\, n_c \cdot v_P = -\Delta P_{P\|} \qquad (3)$$

and the final longitudinal recoil-ion momentum directly reflects the Q-value of the reaction i.e. the difference in the binding energies of the electrons in the initial and final state. In this manner electron capture cross sections from He targets have been investigated as a function of the final state of the captured electron(s) and state selective cross sections have been accessible for the first time at large projectile velocities where traditional energy-gain or -loss techniques are hardly applicable. In addition, $P_{R\perp} = P_{P\perp}$ is exactly fulfilled since only two particles are in final continuum states and the projectile scattering is accessible with high accuracy (pioneering work was done at Kansas State University[27], at Frankfurt[32] and at CAEN[41]).

As a recent example the longitudinal momentum spectrum is shown in Fig. 7 for single electron capture by 10 MeV F^{8+} on He measured at the Kansas State University[66] (for similar collision systems results have been obtained in RIKEN by Kambara and co-workers[39,67]). A resolution in the longitudinal momentum (denoted as P_z in the figure) of $\Delta P_z = 0.15$ a.u. has been achieved, which, at this collision velocity (4.58 a.u.) corresponds to an energy resolution of 18 eV. To achieve an equivalent resolution by measuring the projectile energy gain would require a fractional precision in the determination of the projectile energy change of 10^{-6} which is clearly not possible. The final states which have been found to be populated are n=3 and higher. Capture into K and L shells is nearly negligible at this energy. The energy resolution of 18 eV is good enough to distinguish between pure capture and reaction channels where the remaining He^{1+} ion is excited into any state $n \geq 2$.

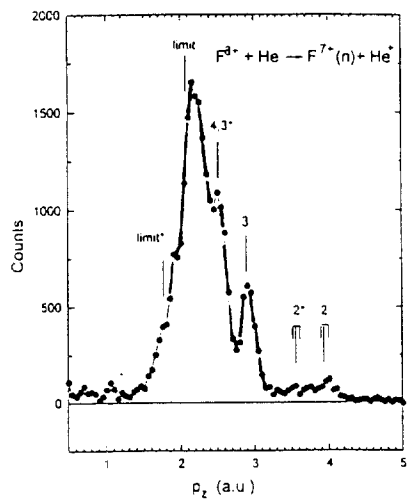

Figure 7: Longitudinal momentum spectrum[66] for 10 MeV F^{8+} + He producing F^{7+} + He^{1+}. The final n of the captured electron is indicted; the * denotes the expected location of capture accompanied by excitation of the He^{1+} ion to $n \geq 2$.

At low energies systematic studies have been performed at the CIRIL by Cassimi and co-workers for various collision systems[41,68] (see also very recent results from KSU[66]). In Fig. 8 doubly differential cross sections for autoionising double electron capture are shown as a function of the projectile energy gain and the scattering angle for 150 keV Ne^{10+} on He collisions. The calculated energy centroids of various doubly excited states as well as expected classical deflection angles for one-step (circles), two-step via n = 4 (squares) and three-step via n = 5 (triangles) transitions are indicated. Simultaneously, doubly differential cross sections have been measured for radiatively stabilised double electron capture and significant differences in the primary populated doubly excited states for both channels have been observed. Whereas stabilised double electron capture mainly populates $Ne^{8+}(4,4)$ states, the population in the autoionising channel is much more complex: An important population of the $Ne^{8+}(4,5)$ and $Ne^{8+}(4,6)$ states as well as significant contribution of the $Ne^{8+}(3,n)$ series has been observed.

Since the projectile energy gain and angular scattering itself is not analysed but only the recoil-ion longitudinal and transverse final momentum is measured to obtain the inelasticity of the reaction, autoionisation of the projectile after the primary population of doubly excited states does not hamper the precision of the measurement. Thus, RIMS presents itself as an ideal tool to investigate these reaction channels, even at low collision velocities as a complementary technique to traditional energy gain or loss techniques.

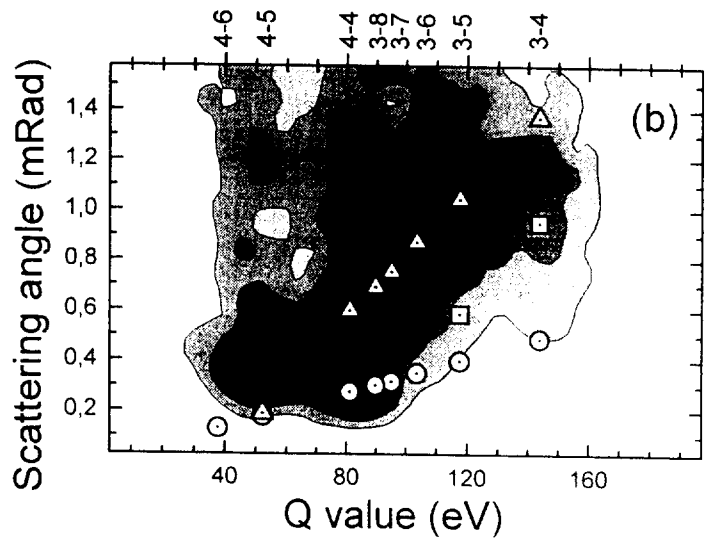

Figure 8: Experimental doubly differential cross sections for autoionising double electron capture in 150 keV Ne^{10+} on He collisions[68] (see text).

4.3 Double Photoionisation

Another example where recoil-ion momentum spectroscopy has enabled a new generation of experiments with respect to completeness, selectivity, and energy range that can be covered, is the ionising interaction by photons with target atoms - a field which experienced a rapid development over the past decade due to the tremendous increase in brilliance of synchrotron radiation facilities (for a detailed overview of the field the reader is referred to the work of Schmidt[69]).

Up to now RIMS has been used to explore double ionisation of helium using photons with energies from about the double ionisation threshold at 80 eV to 58 keV, i.e. over the whole energy range available at modern synchrotron radiation sources. Due to its fundamental nature, as the most simple collision induced multiple ionisation reaction and the extreme sensitivity of the cross sections on the details of the electron-electron interaction, double photoionisation of helium has been the subject of outstanding intense experimental and theoretical research activities during the last several years. Mapping the complete momentum vector of the recoiling target ion after photoionisation at high γ-energies allowed for the first time to separate contributions from Compton scattering and photoabsorption to helium single and double ionisation[43,44] (see Fig. 5). At low and medium energies the complete determination of the ionisation kinematics enabled unprecedented accurate measurements of total cross section ratios by integrating of over all recoil-ion momenta[70].

In this article the kinematically complete (γ,2e) experiment on helium double ionisation by 80 eV photons performed by Dörner and co-workers[49] is shortly described. For a detailed discussion of a complete data set, visualising for the first time the entire final 9-dimensional momentum space without any restrictions in relative emission angles and energies of the emerging three particles at 1,6 and 20 eV above the double ionisation threshold see Dörner et al[71]. To elucidate the mechanisms of the three-body break-up 1 eV above the double ionisation threshold Dörner and coworkers choose Jacobian momentum coordinates, i.e. $\mathbf{k_r} = \mathbf{k_1} + \mathbf{k_2}$ and $\mathbf{k_R} = ½ (\mathbf{k_1} - \mathbf{k_2})$ of the electron centre-of-mass motion and the electron-pair motion, respectively ($\mathbf{k_1}$, $\mathbf{k_2}$ are the momenta of electron 1 and 2, respectively). Neglecting the incoming photon momentum the measured recoil-ion momentum is equal to $-\mathbf{k_r}$ and the electrostatic dipole operator is $\boldsymbol{\varepsilon}\cdot\mathbf{r}$ with $\mathbf{r} = ½(\mathbf{r_1} + \mathbf{r_2})$. In Fig. 9 the momentum distributions for $\mathbf{k_r}$ (the motion of the recoil-ion), $\mathbf{k_1}$ (the motion of either electron) and for $\mathbf{k_R}$ (the relative motion of the two electrons) are projected onto the y-z plane for -0.1 a.u. $< k_x <$ +0.1 a.u. where z is along the photon polarisation vector and y is perpendicular to $\boldsymbol{\varepsilon}$ and to the direction of the incoming photon propagation along x. The He^{2+} recoil-ion distribution qualitatively displayed a dipole distribution whereas such a behaviour was found to be completely washed out in the momentum distribution of either electron due to the strong interaction of both electrons in the final state Fig. 9b)[72,73]. The relative motion of the two electrons (Fig. 9c), however, showed a dis-

tinct pattern indicating that the pair preferentially separates perpendicular to the photon polarisation axis and, thus, to the recoil-ion motion.

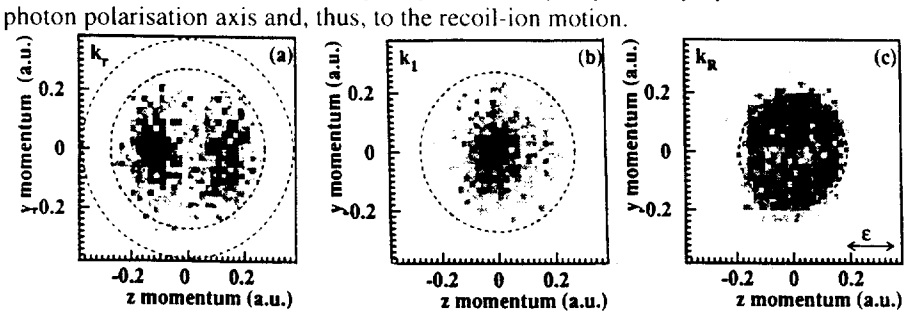

Figure 9: Density plots of projections of the momentum spectra from double ionisation of He by 80.1 eV photons (see text). The polarisation vector of the photons is in the z direction and the photon propagates in the x direction. Only events with -0.1 a.u. < k_x < 0.1 a.u. are projected onto the plane. (a) The He^{2+} recoil-ion (or $-\mathbf{k_r}$) momentum distribution. The outer circle indicates the maximum possible recoil-ion momentum, and the inner circle is the locus of events for which the $\mathbf{k_r}$ motion has half of the excess energy. (b) The distribution of single electron momenta ($\mathbf{k_1}$ or $\mathbf{k_2}$). The circle locates the momentum of an electron which caries the full excess energy. (c) The relative electron momentum (or $\mathbf{k_R} = \mathbf{k_1} - \mathbf{k_2}$) distribution. The circle identifies the maximum possible value for k_R.

The discussion and clear interpretation of the experimental data in terms Jacobian momentum coordinates[74-76] highlight a further advantage of experiments performed using reaction microscopes. Since the full solid angle is covered for all of the fragments in kinematically complete experiments, this allows a transformation of the experimental data to any set of suitable collective coordinates. Such coordinates quite often elucidate the characteristics of the correlated many-body motion in a much more natural, intuitive and better adapted way, as has been demonstrated frequently in nuclear, molecular or solid state physics.

4.4 Double Ionisation by Ion Impact

Double ionisation of helium in collisions with bare projectiles is the most simple charged-particle-induced multiple ionisation reaction. Its investigation is fundamental for the understanding of the role of static and dynamic electron-electron correlation in multi-electron transitions and therefore has been central to many experimental and theoretical ion-atom research activities. Despite of its basic importance, mainly total cross section measurements were performed (for an overview see Refs. 7,77) and only a few investigations differential in the momentum of one of the emitted particles have been reported in literature (for an overview see Ref. 78). No kinematically complete measurements have been feasible up to now due to the enormous difficulties to analyse the final momenta of three emerging particles in coincidence applying conventional spectroscopy for the electrons and the ions.

Using the reaction microscope with three independent electron detectors as shown in Fig. 3, a pioneering kinematically complete experiment on helium double

ionisation by 3.6 MeV/u Se^{28+} impact has been performed recently at GSI [45]. As observed for single ionisation the momentum transfer by the projectile in each individual ionisation reaction was found to be negligibly small compared to the measured final momenta of the recoil ion and the electrons. These recoil-ion and electron momenta consequently have been considered to result from the bound state electron momentum distribution of the helium atom in the initial state. Therefore, both should closely reflect the correlated longitudinal sum-momentum distribution of the electrons in the initial state, i.e. the two-electron Compton profile. Like for single ionisation the fast projectile was observed to deliver energy but only little momentum.

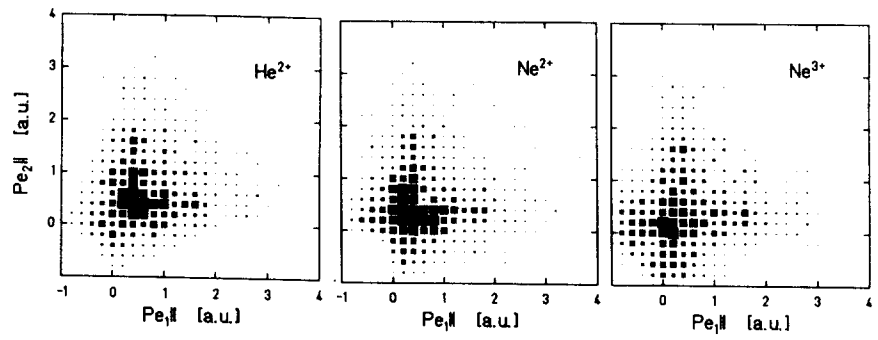

Figure 10: $p_{e1\|}$ versus $p_{e2\|}$ of the two electrons emitted for double ionisation of helium (left part), Ne double (middle part) and Ne triple ionisation (right part) for 3.6 MeV/u Se^{28+} impact[46]. Different box sizes represent the cross sections $d^2\sigma^{2+}/dp_{e1\|}\,dp_{e2\|}$ in $1.0 \cdot 10^{-16}$ $cm^2/a.u.^2$ (largest box) on a linear scale for helium. Results for neon are scaled on the maximum differential cross sections, respectively.

In Fig. 10 the correlated two-electron emission is shown by plotting the the longitudinal momenta of both electrons ($P_{e1\|}$-versus-$P_{e2\|}$) integrated over all recoil-ion transverse and longitudinal momenta (left figure). A distinct pattern is found: if one electron is slow the other one most likely is fast. This feature is even more pronounced for neon double and triple ionisation (middle and right part of the figure). In a series of classical model calculations it was demonstrated that a reasonable, but still not perfect description of the experimental result was only obtained when the $1/r_{12}$ electron-electron interaction was explicitly included after both electrons had a positive energy relative to the target nucleus (double ionisation).

Again one can understand these results by viewing the attosecond ($\sim 10^{-18}$ sec), extremely intense ($\sim 10^{18}$ W/cm^2) electromagnetic pulse which is generated by the passing highly-charged projectile as a field of virtual quanta (Weizäcker-Williams formulation for the ionisation by relativistic projectiles). In this picture each one of the both (three) He(Ne)-electrons is independently „photoionised" by absorbing one virtual photon with an energy corresponding to the individual electron momentum at

the instant of ionisation. A negligibly small momentum is transferred and no significant momentum exchange between the electrons themselves or between each electron and the helium nucleus may take place since the collision time is short compared to the electron revolution time in the bound state. Thus, one can conclude that the initial state correlation evolves in a dynamically controlled way into the continuum and is finally observed in the strongly correlated two-(three)-electron - continuum. Recently, systematic quantum mechanical calculations have been performed by Keller and co-workers[65] on the basis of these considerations for He double ionisation by 3.6 MeV/u Se^{28+} and 2 GeV/u U^{92+} impact. Their results indicate that the details of the ground state electron-electron momentum correlation is visible in the final correlated two-electron state.

5. Summary

Recoil-Ion Momentum Spectroscopy, the determination of the charge state and of the momentum vector of a recoiling target ion emerging from an ionising collision of an atom with any kind of radiation is a technique that has been developed over more than a decade from the first successful experiments to present high-resolution „reaction microscopes". A decisive breakthrough was marked by the implementation of (pre-cooled) supersonic jet targets yielding superior recoil-ion momentum resolution at a 4π detection solid angle for target ions emerging from a large variety of collision induced atomic reactions. Recently, a further substantial improvement was achieved by the invention of rigorously new projection techniques for the detection of electrons and the implementation of such analysers into high-resolution RIM spectrometers. The newest instruments of this kind, termed „reaction microscopes" enable one to determine the momentum vectors of up to four reaction products (the recoil-ion and three emitted electrons) with solid angles exceeding those of conventional methods by many orders of magnitude.

In essence, these two technical innovations initialised a new generation of atomic collision experiments unprecedented in resolution, completeness and broadness covering the entire range of different projectiles (ions, photons, electrons and antiparticles) and collision velocities available at advanced accelerator and synchrotron radiation facilities. Some outstanding examples are: 1. The first kinematically complete experiments for single and double ionisation of atoms by ion impact at GeV energies. 2. The mapping of the two-dimensional final electron momentum space in low energy (5-15 keV) proton helium collisions for defined internuclear impact parameter and collision plane. 3. The imaging of the complete 9-dimensional momentum space after double photoionisation of helium at energies close to threshold. 4. The first experimental separation of the contributions of Compton scattering and photoabsorption to helium double ionisation at keV photon energies.

As the most advanced reaction microscopes have only been in operation for about two years the experimental results reviewed in this paper can certainly be considered as being the fascinating starting point of a large series of kinematically complete experiments to be performed in the near future. One might envisage a variety of exciting results on the dynamics of many-electron transitions and of the electron-electron correlation in atomic collisions but also impact on neighbouring fields like atomic structure investigations for heavy few-electron systems, multi-photon ionisation in strong laser fields, or the collision induced disintegration of molecules. It has been pointed out[79] that the technique might even be profitable for the investigation of the electroweak interaction: kinematically complete β-decay experiments should enable high-precision electron-neutrino angular correlation measurements and, in the far future, a precise neutrino mass determination.

Acknowledgement

The experimental methods and physical interpretations described in this article evolved over more than 10 years from continuous discussions with many colleagues which are too numerous to acknowledge individually. The work was supported by BMBF, GSI and DFG.

References

1. S. Yu. Ovchinnikov and J. H. Macek, *Phys. Rev. Lett.* **75**, 2474 (1995)
2. R. Schultz, Krstic, C.O. Reinhold and J.C. Wells *Phys. Rev. Lett.* **76**, 2882 (1996)
3. A. Lahmam-Bennani, *J. Phys. B* **24**, 2401 (1991)
4. O. Schwarzkopf, B. Krässig, J. Elminger and V. Schmidt, *Phys. Rev. Lett.* **70**, 3008 (1993)
5. A. Huetz, P. Lablanquie, L. Andric, P. Selles, J. Mazeau, *J. Phys. B* **27**, L13 (1994)
6. G. Dawber, L. Avaldi, A.G. McConckey, H. Rojas, M.A. MacDonald M, and G.C. King, *J. Phys. B* **28,** L271 (1995
7. J. McGuire, N. Berrah, R.J. Bartlett, J.A.R. Samson, J.A. Tanis, C.L. Cocke, and A.S. Schlachter, *J. Phys. B* **28**, 913 (1995)
8. A. Lahmam-Bennani, C. Dupré, and A. Duguet, *Phys. Rev. Lett.* **63**, 1582 (1989)
9. C.L. Cocke and R.E. Olson, *Physics Reports* **205(4)**, 155 (1991)
10. J. Ullrich, R. Moshammer, R. Dörner, O. Jagutzki, V. Mergel, H. Schmidt-Böcking, L. Spielberger *J. Phys. B* **30,** 2917 (1997)
11. N.V. Federenko, and V.V. Afrosimov, *Sov. Phys. Tech. Phys.* **1**, 1872 (1956)
12. E. Everhart, and Q.C. Kessel, *Phys. Rev. Lett.* **14**, 247 (1965)
13. J. W. McConckey, A. Crowe, and M. A. Hender *Phys. Rev. Lett.* **29**, 1 (1972)
14. J. C. Levin, R.T. Short, C.S. O, S.B. Elston, J.P. Gibbons, I.A. Sellin, and H. Schmidt-Böcking, *Phys. Rev. A* **36**, 1649 (1987)
15. R.E. Olson, J. Ullrich, and H. Schmidt-Böcking, *J. Phys. B* **20**, L809 (1987)
16. J.P. Grandin, D. Hennecart, X. Husson, D. Lecler, I. Lesteven-Vaisse, and D. Lisfi, *Europhys. Lett.* **6(8)**, 683 (1988)
17. J. Ullrich, and H. Schmidt-Böcking, *Phys. Lett. A* **125**, 193 (1987)
18. J. Ullrich, H. Schmidt-Böcking, and C. Kelbch, *Nucl. Inst. Meth. A* **268**, 216 (1988)

19. J. Ullrich, R. Dörner, S. Lencinas, O. Jagutzki, and H. Schmidt-Böcking, *Nucl. Inst. Meth. B* **61**, 415 (1991)
20. R. Dörner, J. Ullrich, H. Schmidt-Böcking, and R.E. Olson, *Phys. Rev. Lett.* **63**, 147 (1989)
21. J. Ullrich, M. Horbatsch, V. Dangendorf, S. Kelbch, and H. Schmidt-Böcking, *J. Phys. B* **21**, 611 (1988)
22. J. Ullrich, R.E. Olson, R. Dörner, S. Kelbch, H. Berg, and H. Schmidt-Böcking, *J. Phys. B* **22**, 627 (1989)
23. R. Dörner, J. Ullrich, R.E. Olson, O. Jagutzki, and H. Schmidt-Böcking, *Phys. Rev. A* **47**, 3845 (1993)
24. E. Forberich, R. Dörner, J. Ullrich, R.E. Olson, K. Ullmann, A. Gensmantel, S. Lencinas, O. Jagutzki, and H. Schmidt-Böcking, *J. Phys. B* **24**, 3613 (1991)
25. A. Gensmantel, J. Ullrich, R. Dörner, R.E. Olson, K. Ullmann, E. Forberich, S. Lencinas, and H. Schmidt-Böcking, *Phys. Rev. A* **45**, 4572 (1992)
26. S. Lencinas, J. Ullrich, R. Dörner, R.E. Olson, W. Wolff, H. Wolff , L. Spielberger, S. Hagmann, M. Horbatsch, C.L. Cocke, H. Schmidt-Böcking, *J. Phys. B* **26**, 287 (1993)
27. I. Ali, V. Frohne, C.L. Cocke, M. Stöckli, S. Cheng, and L.A. Raphaelian, *Phys. Rev. Lett.* **69**, 2491 (1992)
28. V. Frohne, S. Cheng, R. Ali, M. Raphaelian, C.L. Cocke, and R.E. Olson, *Phys. Rev. Lett.* **71**, 696 (1993)
29. V. Frohne, S. Cheng, R. Ali, M. Raphaelian, C.L. Cocke, and R.E. Olson, *Phys. Rev. A* **53**, 2407 (1996)
30. P. Jardin, J.P. Grandin, A. Cassimi, J.P. Lemoigne , A. Gosselin, X. Husson, D. Hennecart, A. Lepontre, *5th Conference on Atomic Physics of Highly Charged Ions*, AIP Conference Proceedings **274**, 291 (1993)
31. O. Jagutzki, PhD-thesis, Johann-Wolfgang-Goethe Universität Frankfurt, published in Edition Wissenschaft, Reihe Physik, Bd.1 Tectum Verlag, Marburg (1995)
32. V. Mergel, R. Dörner, J. Ullrich, O. Jagutzki, S. Lencinas, S. Nüttgens, L. Spielberger, M. Unverzagt, C.L. Cocke, R.E. Olson, M. Schulz, U. Buck, E. Zanger, W. Theisinger, M. Isser, S. Geis, and H. Schmidt-Böcking, *Phys. Rev. Lett.* **74**, 2200 (1995)
33. R. Moshammer, J. Ullrich, M. Unverzagt, W. Schmitt, P. Jardin, R.E. Olson, R. Mann, R. Dörner, V. Mergel, U. Buck, and H. Schmidt-Böcking, *Phys. Rev. Lett.* **73**, 3371 (1994)
34. R. Dörner, V. Mergel, L. Spielberger, O. Jagutzki, M. Unverzagt, W. Schmitt , J. Ullrich, R. Moshammer, H. Khemliche, M. Prior, R.E. Olson, L. Zhaoyuan L, W. Wu, C.L. Cocke, and H. Schmidt-Böcking, in *The Physics of Electronic and Atomic Collisions* AIP Conference Proceedings **360**, 495 (1995)
35. R. Dörner, V. Mergel, R. Ali, U. Buck, C.L. Cocke, K. Froschauer, O. Jagutzki, S. Lencinas, W.E. Meyerhof, S. Nüttgens, R.E. Olson, H. Schmidt-Böcking, L. Spielberger, K. Tökesi, J. Ullrich, M. Unverzagt, and W. Wu, *Phys. Rev. Lett.* **72**, 3166 (1994)
36. W. Wu, K.L. Wong, R. Ali, C.L. Cocke, V. Frohne, J.P. Giese, M. Raphaelian, B. Walch, R. Dörner, V. Mergel, H. Schmidt-Böcking, and W.E. Meyerhof, *Phys. Rev. Lett.* **72**, 3170(1994)
37. W. Wu, J.P. Giese, Z. Chen, R. Ali, C.L. Cocke, P. Richard, and M. Stöckli, *Phys. Rev. A* **50**, 502 (1994)
38. W. Wu , K L. Wong, C.L. Cocke, J.P. Giese, and E.C. Montenegro, *Phys. Rev. A* **51**, 3718 (1995)
39. T. Kambara, J.Z. Tang, Y. Awaya, B.D. DePaola, O. Jagutzki, Y. Kanai, M. Kimura, T.M. Kojima, V. Mergel, Y. Nakai, H. Schmidt-Böcking, I. Shimamura, *J. Phys. B* **28**, 4593-4606 (1995)
40. M. Abdallah, C.L. Cocke, S Kravis, E.C. Montenegro, R. Moshammer, L. Salesh, J. Ullrich, S.L. Varghese, W. Wolff, and H. Wolff, *Nucl. Instr. Meth.* (accepted for publication)
41. A. Cassimi, S. Duponchel, X. Flechard, P. Jardin, P. Sortais, D. Hennecart, and R.E. Olson, *Phys. Rev. Lett.* **76**, 3679 (1996)

42. V. Mergel, R. Dörner, M. Achler, Kh. Khayyat, S. Lencinas, J. Euler, O. Jagutzki, S. Nüttgens, M. Unverzagt, L. Spielberger, W. Wu, R. Ali, J. Ullrich, H. Cederquist, A. Salin, C.J. Wood, R.E. Olson, Dz. Belkic, C.L. Cocke, H. Schmidt-Böcking *Phys. Rev. Lett.* **79**, 387 (1997)
43. L. Spielberger, O. Jagutzki, R. Dörner, J. Ullrich, U. Meyer, V. Mergel, M. Unverzagt, M. Damrau, T. Vogt, I. Ali, Kh. Khayyat, D. Bahr, H-G. Schmidt, R. Frahm, and H. Schmidt-Böcking, *Phys. Rev. Lett.* **74**, 4615 (1995)
44. L. Spielberger, O. Jagutzki, B. Krässig, U. Meyer, Kh. Khayyat, V. Mergel, Th. Tschentscher, Th. Buslaps, H. Bräuning, R. Dörner, T. Vogt, M. Achler, J. Ullrich, D.S. Gemmell, and H. Schmidt-Böcking, *Phys. Rev. Lett.* **76**, 4685 (1996)
45. R. Moshammer, M. Unverzagt, W. Schmitt, J. Ullrich, and H. Schmidt-Böcking, *Nucl. Instr. Meth. B* **108**, 425-445 (1996)
46. R. Moshammer, J. Ullrich, H. Kollmus, W. Schmitt, M. Unverzagt, O. Jagutzki, V. Mergel, H. Schmidt-Böcking, R. Mann, C.J. Wood, and R.E. Olson, *Phys. Rev. Lett.* **77**, 1242 (1996)
47. R. Dörner, H. Khemliche, M.H. Prior, C.L. Cocke, J.A. Gary, R.E. Olson, V. Mergel, J. Ullrich, and H. Schmidt-Böcking, *Phys. Rev. Lett.* **77**, 4520 (1996)
48. T. Vogt, R. Dörner, O. Jagutzki, C.L. Cocke, J. Feagin, M. Jung, E.P. Kantr, H. Khemliche, S. Kravis, V. Mergel, L. Spielberger, J. Ullrich, M. Unverzagt, H. Bräuning, U. Meyer, and H. Schmidt-Böcking, *Proceedings of the Euroconference on (γ,2e) and (e,2e) Reactiions*, Plenum (1997), (accepted)
49. R. Dörner, J.M. Feagin, C.L. Cocke, H. Bräuning, O. Jagutzki, M. Jung, E.P. Kanter, H. Khemliche, S. Kravis, V. Mergel, M.H. Prior, H. Schmidt-Böcking, L. Spielberger, J. Ullrich, M. Unverzagt, and T. Vogt, *Phys. Rev. Lett.* **77**, 1024 (1996)
50. H. Kollmus, W. Schmitt, R. Moshammer, M. Unverzagt, and J. Ullrich, *Nucl. Inst. Meth. B* **124**, 377 (1996)
51. S.E. Sobottka and M.B. Williams, IEEE *Trans. on Nucl. Science* **35**, 3481(1988)
52. S. Nüttgens, diploma-thesis, Universität Frankfurt (1994)
53. H. Schmidt-Böcking, R. Dörner, J. Ullrich, J. Euler, H. Berg, E. Forberich, S. Lencinas, O. Jagutzki, A. Gensmantel, K. Ullmann, R.D. DuBois, Jiazhen Feng, R.E. Olson, A. Gonzáles, and S. Hagmann, in *Lecture Notes in Physics* **376**, 268 (1990) (Springer Verlag)
54. V. Rodríguez, Y.D. Wang, and C.D. Lin, *Phys. Rev. A* **52**, R9 (1995)
55. V. Mergel, *„Dynamische Elektronenkorrelation in Helium"*, Shaker Verlag, Aachen (1996)
56. T. Vogt, diploma-thesis, Universität Frankfurt (1996)
57. R. Dörner, V. Mergel, L. Spielberger, M. Achler, Kh. Khayyat, T. Vogt, H. Bräuning, O. Jagutzki, J. Ullrich, R. Moshammer, M. Unverzagt, W. Schmitt, H. Khemliche, M.H. Prior, C.L. Cocke, J. Feagin, R.E. Olson, and H. Schmidt-Böcking, *Nucl. Inst. Meth. B* **124**, 225 (1997)
58. R. Moshammer, J. Ullrich, H. Kollmus, W. Schmitt, M. Unverzagt, H. Schmidt-Böcking, C.J. Wood, and R.E. Olson, *Phys. Rev. A* (1997) (accepted)
59. V. Rodríguez, Y.D. Wang, and C.D. Lin, *J. Phys. B* **28**, L471 (1995)
60. S. F.C. O'Rourke and D.D.F. Crothers, *J. Phys. B* **30**, 2443 (1997)
61. R. Moshammer et al., *GSI Annual Report 1996* GSI-1997-1, p. 105
62. P. Jardin, A. Cassimi, J.P. Grandin, H. Rothard, J.P. Lemoigne, D. Hennecart, X. Husson, A. Lepontre, *Nucl. Inst. Meth. B* **107**, 41 (1996)
63. M. Unverzagt, R. Moshammer, W. Schmitt, R.E. Olson, P. Jardin, V. Mergel, J. Ullrich, and H. Schmidt-Böcking, *Phys. Rev. Lett.* **76**, 1043 (1996)
64. R. Moshammer, J. Ullrich, H. Kollmus, W. Schmitt, M. Unverzagt and H. Schmidt-Böcking, Proceedings of the *17th International Conference on X-ray and Inner-Shell Processes* (1996) (accepted)
65. S. Keller, H.J. Lüdde, and R.M Dreizler *Phys. Rev. A* **55**, 4215 (1997)
66. M. Abdallah, C.L. Cocke, S. Kravis, E.C. Montenegro, R. Moshammer, L. Saleh, J. Ullrich, S.L. Varghese, W. Wolff, and H. Wolf, *American Institute of Physics*, (1997) (accepted)
67. T. Kambara, A. Igarashi, N. Watanabe, Y. Nakai, T.M Kojima, and Y. Awaya, *J. Phys. B* **30**, 1251 (1997)

68. X. Flechard, S. Duponchel, L. Adoui, A. Cassimi, P. Roncin, and D. Hennecart, *J. Phys. B* (1997) (submitted)
69. V. Schmidt, *Rep. Prog. Phys.* **55**, 1483 (1992)
70. R. Dörner, T. Vogt, V. Mergel, H. Khemliche, S. Kravis, C.L. Cocke, J. Ullrich, M. Unverzagt, L. Spielberger, M. Damrau, O. Jagutzki, I. Ali, B. Weaver, K. Ullmann, C.C. Hsu, M. Jung, E.P. Kanter, B. Sonntag, M.H. Prior, E. Rotenberg, J. Denlinger, T.Warwick, S.T. Manson, and H. Schmidt-Böcking, *Phys. Rev. Lett.* **76**, 2654 (1996)
71. R. Dörner, H. Bräuning, V. Mergel, O. Jagutzki, L. Spielberger, T. Vogt, H. Kehmliche, M.H. Prior, J. Ullrich, C.L. Cocke, H. Schmidt-Böcking, *Phys. Rev. A* (1997) (submitted)
72. R. Wehlitz , F. Heiser, O. Hemmers, B. Langer, A. Menzel, and U. Becker, *Phys. Rev. Lett.* **67**, 3764 (1991)
73. G. Dawber, L. Avaldi, A.G. McConckey, H. Rojas, M.A. MacDonald, and G.C. King, *J. Phys. B* **28**, L271 (1995)
74. J.M. Feagin *J. Phys. B* **28**, 1495 (1995)
75. J.M. Feagin *J. Phys. B* **29**, 1551 (1996)
76. M. Pont and R. Shakeshaft *Phys. Rev. A* **54**, 1448 (1996)
77. J. McGuire, *Adv. At. Phys.* **29**, 217 (1991)
78. J. Ullrich, GSI-EPORT, GSI-94-08 (1994) in German
79. J. Ullrich, R. Dörner, V. Mergel, O. Jagutzki, L. Spielberger and H. Schmidt-Böcking, *Comments At. Mol. Phys.* **30(5)** 285